Journal of Power Sources 195 (2010) 6652–6658

Contents lists available at ScienceDirect

Journal of Power Sources

journal homepage: www.elsevier.com/locate/jpowsour

Mathematical modeling analysis of regenerative solid oxide fuel cells in switching mode conditions

Xinfang Jin, Xingjian Xue*

Department of Mechanical Engineering, University of South Carolina, Columbia, SC 29208, USA

ARTICLE INFO

Article history:
Received 25 February 2010
Received in revised form 6 April 2010
Accepted 7 April 2010
Available online 13 April 2010

Keywords:
Mathematical model
Transient
Regenerative SOFC
Electrolysis

ABSTRACT

A 2D transient mathematical model is developed for regenerative solid oxide cells operated in both SOFC mode and SOEC mode. The steady state performance of the model is validated using experimental results of in-house prepared NiO–YSZ/YSZ/LSM cell under different operating temperatures. The model is employed to investigate complicated multi-physics processes during the transient process of mode switching. Simulation results indicate that the trend of internal parameter distributions, including $H_2/O_2/H_2O$ and ionic potentials, flip when the operating cell is switched from one mode to another. However, the electronic potential shows different behaviors. At H_2 electrode, electronic potential keeps at zero voltage level, while at O_2 electrode, it increases from a relatively low level in SOFC mode to a relatively high level in SOEC mode. Transient results also show that an overshooting phenomenon occurs for mass fraction distribution of water vapor at H_2 side when the operating cell switches from SOFC mode to SOEC mode. The mass fractions of O_2 and H_2 as well as charge (electrons and ions) potentials may quickly follow the operating mode changes without over-shootings. The simulation results facilitate the internal mechanism understanding for regenerative SOFCs.

Published by Elsevier B.V.

1. Introduction

Solid oxide fuel cell (SOFC) is one of the promising clean energy technologies that convert the chemical energy of hydrogen into electronic energy directly [1]. Mathematical modeling technique has been proved a cost effective method in fundamental mechanism understanding and optimization designs of SOFCs at different levels. In this respect, steady state models have been developed extensively to study various internal parameter distributions including heat transfer, mass transport, charge migration, and electrochemical reactions and their links to SOFC performances [2–6]. Transient models have also been utilized to investigate SOFC dynamic behaviors [7–14].

The SOFC can also be operated in electrolysis mode, e.g., solid oxide electrolyzer cell (SOEC), where hydrogen/oxygen is generated with the consumption of electricity. In this respect, SOEC models have been developed in literature, most of which are steady state [15–21]; few models can be found for transient performance investigations.

When a solid oxide cell/stack is operated in SOFC mode and SOEC mode alternatively, energy sustainability could be implemented. In this regenerative operating mode, SOFC/SOEC system is able to better utilize and support electricity grid. When grid electricity demand increases, SOFC mode turns on to generate electricity for the grid; when grid electricity demand decreases, SOEC may utilize grid electricity to produce hydrogen. During the switching process between SOFC mode and SOEC mode, there will be very complicated transient interactions between electrochemical reactions and transport processes. The fundamental mechanism understanding under the switching mode will play a significant role for SOFC/SOEC system design and operations. However, no research can be found in open literatures for this purpose.

This paper aims at investigating transient behaviors of SOFC/SOEC in switching mode conditions using mathematical modeling approach. The research considers a general 2-D model that includes flow channels and positive electrode–electrolyte–negative electrode (PEN) assembly. The research goal is to elucidate the complicated interactions among transport and electrochemical processes when the cell is switched from one operating mode to another.

2. Mathematical model

The geometry of a planar 2-D hydrogen electrode supported solid oxide cell is illustrated in Fig. 1, including flow channels and PEN assembly. Since the cell could be operated in either fuel cell mode or electrolysis mode, steam (H_2O) is assumed in both hydro-

* Corresponding author at: Department of Mechanical Engineering, University of South Carolina, 300 Main Street, Room A224, Columbia, SC 29208, USA.
Tel.: +1 803 576 5598; fax: +1 803 777 0106.
E-mail addresses: Xue@cec.sc.edu, xue@engr.sc.edu (X. Xue).

0378-7753/$ – see front matter. Published by Elsevier B.V.
doi:10.1016/j.jpowsour.2010.04.018

Nomenclature

$c_{H_2O,ref}$	reference concentration of water (mol m^{-3})
$c_{H_2,ref}$	reference concentration of hydrogen (mol m^{-3})
c_t	total concentration of species (mol m^{-3})
D_{ij}	the *ij* component of the multicomponent Fick diffusivity (m^2 s^{-1})
F	Faraday's constant (C mol^{-1})
I	the momentum (kg m s^{-1})
$i_{0,H}$	hydrogen electrode exchange current density (A m^{-2})
$i_{0,O}$	oxygen electrode exchange current density (A m^{-2})
$i_{H,ct}$	hydrogen electrode current density (A m^{-2})
$i_{O,ct}$	oxygen electrode current density (A m^{-2})
M_j	molar mass of species *j* (kg mol^{-1})
n_i	number of electrons in the reaction
p	pressure (Pa)
Q	mass source term (kg m^{-3})
R	gas constant (J mol^{-1} K^{-1})
R_i	reaction source term for species *i* (kg m^{-3} s)
S_a	specific surface area (m^{-1})
T	temperature (K)
w_j	mass fraction of species *j*
x	molar fraction

Greek letters

ε	porosity of the medium
η	over voltage (V)
κ	permeability of the medium (m^2)
μ	dynamic viscosity (Pa s)
ν_i	stoichiometric coefficient
ρ	density of the fluid (kg m^{-3})
σ	conductivity of electron or ion (S m^{-1})
ϕ	electric potential (V)
$\Delta\phi_{eq}$	equilibrium potential difference (V)

Subscripts

e	electronic
i	ionic
H	hydrogen
O	oxygen

gen channel and oxygen channel. As a result, gases in hydrogen electrode side are the mixture of H_2 and H_2O while those in oxygen electrode side are the mixture of H_2O, O_2 and N_2. In the model, we assume isothermal conditions; the reactant gas mixtures are approximated as ideal gases; composite electrodes are assumed so that electrochemical reaction sites are uniformly distributed in hydrogen and oxygen electrodes.

For SOFC mode, oxygen flows into oxygen channel and diffuses into porous oxygen electrode, where oxygen molecules combine with electrons coming from external circuit, and forms into oxygen ions. The oxygen ions migrate through the dense electrolyte to the hydrogen electrode. At the hydrogen side, steam and hydrogen flow into the hydrogen channel. The hydrogen then diffuses into porous hydrogen electrode, where hydrogen molecules combine with oxygen ions coming from the oxygen electrode, and form into steam and release electrons. The electrons then transport through external circuit from hydrogen electrode to oxygen electrode. As a result, electricity is generated. When an external voltage, greater than the open circuit potential of a SOFC, is applied to the cell, the SOFC mode of the cell is switched to SOEC mode. In this scenario, the internal transport and electrochemical reactions will reverse. Specifically, steam at the porous hydrogen electrode is split into hydrogen molecules and oxygen ions with a supply of electrons from external circuit. The oxygen ions then migrate via the dense electrolyte to the oxygen electrode, where oxygen ions then form into oxygen molecules and release electrons. The electrons then transport from oxygen electrode to hydrogen electrode through external circuit. During the process, hydrogen and oxygen are produced and electricity is consumed. The corresponding mathematical model, describing the transport and electrochemical processes within a solid oxide cell operated in both SOFC mode and SOEC mode, is detailed as follows.

2.1. Charge balance

Both electronic and ionic transports are allowed in composite electrodes, while electrolyte only allows ions to migrate through. According to the generalized Ohm's law, the governing equations for charge balance can be described as:

$$\nabla(-\sigma_e \nabla\phi_e) = \pm S_a i_{ict} \tag{1}$$

$$\nabla(-\sigma_i \nabla\phi_i) = \pm S_a i_{ict} \tag{2}$$

where σ_e and σ_i are electronic and ionic conductivities, ϕ_e and ϕ_i are electronic and ionic potentials respectively. S_a the effective triple phase boundary (TPB) length. The signs in the right sides of Eqs. (1) and (2) are dependent on the cell mode. In SOFC mode, oxygen electrode serves as ion sources and electron sinks, while hydrogen electrode serves as ion sinks and electron sources. In SOEC mode, the sources and sinks will be reversed.

i_{ict} in Eqs. (1) and (2) is the current density and is represented using Bulter–Volmer equation. For SOFC mode:

$$i_{H,ct} = i_{0,H}\left[x_{H_2}\frac{c_t}{c_{H_2,ref}}\exp\left(\frac{0.5F}{RT}\eta_H\right) - x_{H_2O}\frac{c_t}{c_{H_2O,ref}}\exp\left(\frac{-0.5F}{RT}\eta_H\right)\right] \tag{3}$$

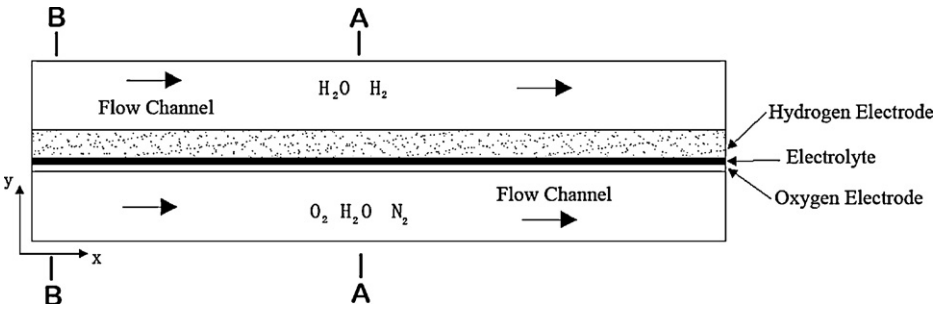

Fig. 1. Schematic of a 2-D planar SOFC.

Table 1
The signs of the equations for SOFC and SOEC modes.

Electrode	Mode			
	SOFC mode		SOEC mode	
	Hydrogen electrode	Oxygen electrode	Hydrogen electrode	Oxygen electrode
$\nabla(-\sigma_1\nabla\phi_{electronic}) = \pm S_a i_{ict}$	−	+	+	−
$\nabla(-\sigma_2\nabla\phi_{ionic}) = \pm S_a i_{ict}$	+	−	−	+
$\eta = \pm(\phi_{electronic} - \phi_{ionic} - \Delta\phi_{eq})$	+	−	−	+
Source term for O_2	N/A	−	N/A	+
Source term for H_2O	+	0	−	0
Source term for N_2	0	0	0	0
Source term for H_2	−	N/A	+	N/A

N/A: not applicable.

$$i_{O,ct} = i_{0,O}\left[x_{O_2}\frac{c_t}{c_{O_2,ref}}\exp\left(\frac{0.5F}{RT}\eta_O\right) - \exp\left(\frac{-0.5F}{RT}\eta_O\right)\right] \quad (4)$$

For SOEC mode,

$$i_{H,ct} = i_{0,H}\left[x_{H_2O}\frac{c_t}{c_{H_2O,ref}}\exp\left(\frac{0.5F}{RT}\eta_H\right) - x_{H_2}\frac{c_t}{c_{H_2,ref}}\exp\left(\frac{-0.5F}{RT}\eta_H\right)\right] \quad (5)$$

$$i_{O,ct} = i_{0,O}\left[\exp\left(\frac{0.5F}{RT}\eta_O\right) - x_{O_2}\frac{c_t}{c_{O_2,ref}}\exp\left(\frac{-0.5F}{RT}\eta_O\right)\right] \quad (6)$$

Here η_H and η_O are overpotentials in H_2 electrode and O_2 electrode respectively. Table 1 provides comprehensive information on how to choose signs for the source terms of governing equations when the cell is operated in SOFC mode and SOEC mode respectively.

2.2. Multicomponent transport

The gas transport is described by the Maxwell–Stefan's diffusion and convection equations:

$$\rho\frac{\partial\omega_i}{\partial t} + \nabla\left(\omega_i\rho u - \rho\omega_i\sum_{j-1}^{k}D_{ij}\left(\frac{M}{M_j}\left(\nabla\omega_j + \omega_j\frac{\nabla M}{M}\right) + (x_j - \omega_j)\frac{\nabla p}{P}\right)\right) = R_i \quad (10)$$

where ω_i is the weight fraction of species i. The source term R_i is determined by the electrochemical reactions according to the Faraday's law [2].

$$R_i = \nu_i\frac{i_{ct,i}M_i}{n_iF} \quad (11)$$

2.3. Gas-flow equations

The weakly compressible Navier–Stokes equations govern the flows in the open channels:

$$\rho\frac{\partial u}{\partial t} + \rho(u\cdot\nabla)u = \nabla\left[-pI + \mu\left((\nabla u + (\nabla u)^T) - \frac{2}{3}(\nabla\cdot u)I\right)\right] \quad (12)$$

$$\frac{\partial\rho}{\partial t} + \nabla\cdot\rho u = Q \quad (13)$$

where μ is the dynamic viscosity and I is the momentum.

In porous electrodes, the Brinkman equation is used to describe the flow:

$$\rho\frac{\partial u}{\partial t} + \left(\frac{\mu}{\kappa} + Q\right)u = \nabla\left[-pI + \frac{\mu}{\varepsilon}\left(\nabla u + (\nabla u)^T - \frac{2}{3}(\nabla\cdot u)I\right)\right] \quad (14)$$

$$\frac{\partial\rho}{\partial t} + \nabla\cdot\rho u = Q \quad (15)$$

where ε and κ denote, respectively, the porosity and permeability of the electrodes and Q, the mass source term, is related to the charge transfer current density:

$$Q = \sum_i S_a\frac{i_{ct,i}M_i}{n_iF} \quad (16)$$

3. Experimental and model validation

The *V–I* curves are first obtained using an in-house prepared cell. In the experimental, the powder mixture of NiO–YSZ and organic additives were dry-pressed into a pellet as hydrogen electrode substrate. A layer of YSZ powder was put on the surface of the substrate, co-pressed to form bilayer structure consisting of hydrogen electrode and electrolyte. The bilayer structure was then sintered at 1450 °C in air for 5 h. The $La_{0.8}Sr_{0.2}MnO_3$ (LSM) powders synthesized by a glycine-nitrate process (GNP) were intimately mixed and ground with fine YSZ powders and organic additives to form an ink, with which the YSZ electrolyte surface of the YSZ/NiO–YSZ bilayer was painted and fired at 1250 °C for 2 h to form oxygen electrode. The obtained button cell has a diameter of 12 mm, oxygen electrode area of 0.35 cm^2, hydrogen electrode thickness of 400 μm, electrolyte thickness of 30 μm and oxygen electrode thickness of 50 μm, respectively. The cell was then tested in both SOFC mode and SOEC mode. In SOFC mode, the mixture of 70% vol H_2 and 30% H_2O was used as a fuel, the ambient air as the oxidant. After sweeping a *V–I* curve in SOFC mode, the applied voltage increased so that SOFC mode was switched to SOEC mode. The corresponding *V–I* curves were recorded in different temperature conditions as shown in Fig. 2.

The mathematical model is solved using COMSOL Multiphysics 3.5. The physical parameters used in the model are summarized in Table 2. The parameters denoted by "b" are difficult to determine in the experiment and are used as adjustable parameters to fit the model predictions with experimental results. As shown in Fig. 2, the simulation results agree very well with experimental results. The overall consistency between the experimental data and the simulated results indicates that the present model is reasonable. While the model may need further validation for general planar solid oxide cells, the physical parameters obtained here will be employed for numerical analysis in different cell geometry dimensions.

Table 2
Physical parameters used in the model.

Parameters	Values	Explanations
d_H[a]	6.0×10^{-4} (m)	Thickness of hydrogen electrode
d_O[a]	1.0×10^{-4} (m)	Thickness of oxygen electrode
$d_{electrolyte}$[a]	1.0×10^{-4} (m)	Thickness of electrolyte
$d_{channel}$	1.0×10^{-3} (m)	Thickness of the channel
L_{cell}[a]	0.019 [m]	Length of the cell
ξ	0.3	Volumetric fraction of ion conductor
ε	0.4	Porosity
σ_i	$33{,}400 \times \exp(-10\,300/T) \times \xi$ (S m^{-1})	Ionic conductivity
$\sigma_{e,H}$	$2 \times 10^6 \times (1-\varepsilon-\xi)$ (S m^{-1})	Electronic conductivity in H_2 electrode
$\sigma_{e,O}$	$(4.2 \times 10^6)/T \exp(-11{,}500/T) \times (1-\varepsilon-\xi)$ (S m^{-1})	Electronic conductivity in O_2 electrode
$\sigma_{i,electrolyte}$	$33{,}400 \times \exp(-10{,}300/T) \times \xi$ (S m^{-1})	Electrolyte conductivity
$i_{0,H}$[b]	1 (A m^{-2})	Exchange current density in H_2 electrode
$i_{0,O}$[b]	0.1 (A m^{-2})	Exchange current density in O_2 electrode
S_a[b]	10^9 (m^{-1})	Specific surface area

[a] 2-D planar SOFC geometry dimensions for simulations in switching mode conditions.
[b] The parameters are adjustable.

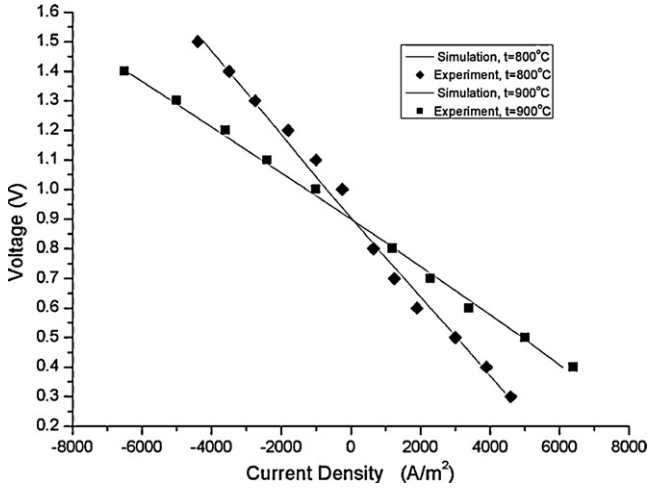

Fig. 2. Comparisons of model predictions with experimental results.

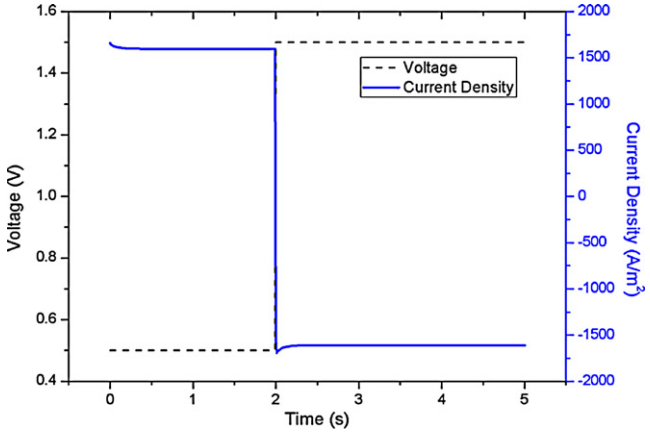

Fig. 3. Transient responses of voltage and current density in switching mode.

4. Results and discussions

In general, it is very difficult for experimental method to measure internal transport and reaction processes within solid oxide cells, especially during the transient process of operating mode switching. The mathematical model developed above will be employed to investigate these performances. In the simulation, the cell is first operated under SOFC mode with the cell voltage setting at 0.5 V. At the time of 2 s, the cell voltage is subject to a sudden step change from 0.5 to 1.5 V, as a result, the cell SOFC mode is changed to SOEC mode. Correspondingly, the cell current density decreases from 1700 A m^{-2} at SOFC mode to -1600 A m^{-2} at SOEC mode as shown in Fig. 3.

The hydrogen and oxygen mass fraction distributions are shown in Fig. 4 when the cell is in the corresponding steady state conditions of SOFC mode and SOEC mode. It can be seen from Fig. 4(a) that both the hydrogen and oxygen decrease along the flow directions when the cell is in SOFC mode, where the hydrogen/oxygen are consumed due to electrochemical reactions. Once the cell is switched to SOEC mode, the corresponding hydrogen/oxygen mass fraction distributions increase, as shown in Fig. 4(b).

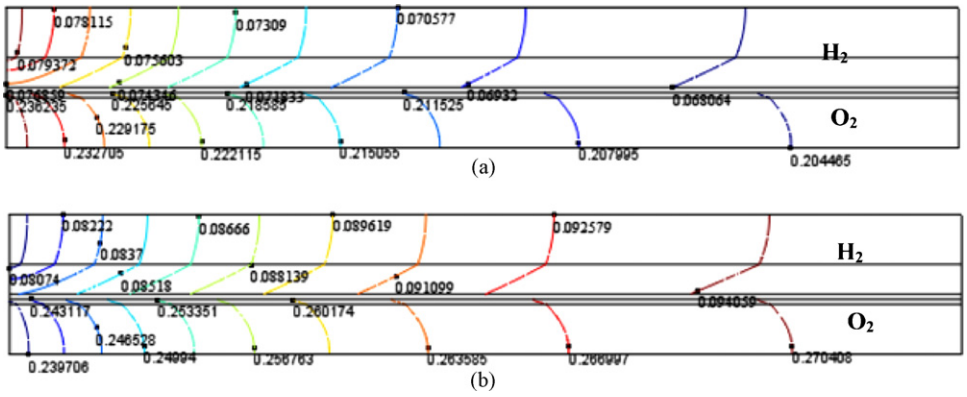

Fig. 4. Hydrogen and oxygen mass fraction distributions (a) SOFC mode; (b) SOEC mode.

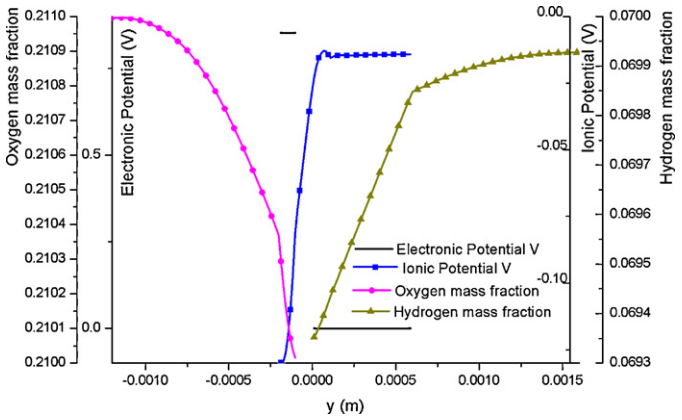

Fig. 5. Parameter distributions along A–A at the 2nd second.

In order to examine the internal transport process changes induced by the sudden step increasing of cell voltage, the internal parameter distributions are obtained along a line parallel to y-axis at $x = 0.009$ m (line A–A as shown in Fig. 1). At the time of 2 s, the cell is in SOFC mode, the corresponding parameter distributions are shown in Fig. 5. Due to the hydrogen and oxygen consumptions by electrochemical reactions, hydrogen and oxygen mass fractions decrease from respective channels towards electrode/electrolyte interfaces. At the oxygen electrode, ionic potential increases from channel/electrode interface towards the electrode/electrolyte interface. Within the electrolyte, ionic potential keeps increasing from oxygen electrode side towards hydrogen electrode side. At hydrogen electrode, ionic potential is around −0.0125 V with a slight variation. The electronic potential keeps at 0 V level at H_2 electrode while reaching 0.87 V at O_2 electrode in SOFC mode.

Once the cell voltage is increased to 1.5 V, the SOFC mode is switched to SOEC mode. The corresponding parameter distributions are shown in Fig. 6. Since H_2 and O_2 are generated in SOEC mode, the trend of corresponding mass fractions flips when compared to those in Fig. 5, which increase from channels towards electrode/electrolyte interface along the A–A. The ionic potential distribution also shows an opposite trend to that in Fig. 5. The electronic potential is 0 V at H_2 electrode, but reaches about 1.15 V at O_2 electrode. Obviously, except for electronic potential, the rest of parameter distributions show opposite trend to those in Fig. 5.

Fig. 7 shows the evolution history of O_2 mass fraction distribution along the line parallel to y-axis at $x = 0.002$ m (line B–B in Fig. 1) during the transient process of cell mode switching. At the 1.99th second, the cell is in SOFC mode, O_2 mass fraction decreases

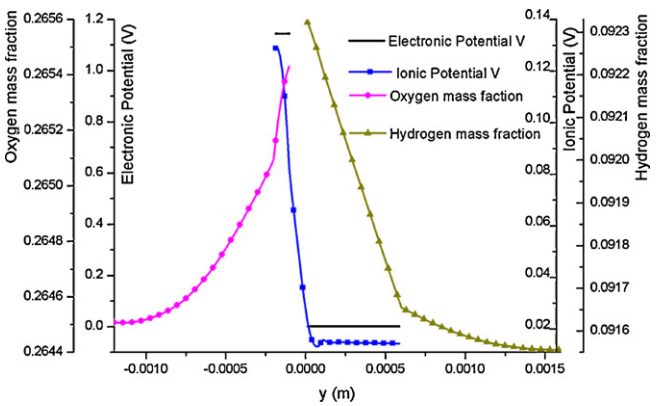

Fig. 6. Parameter distributions along A–A at the 5th second.

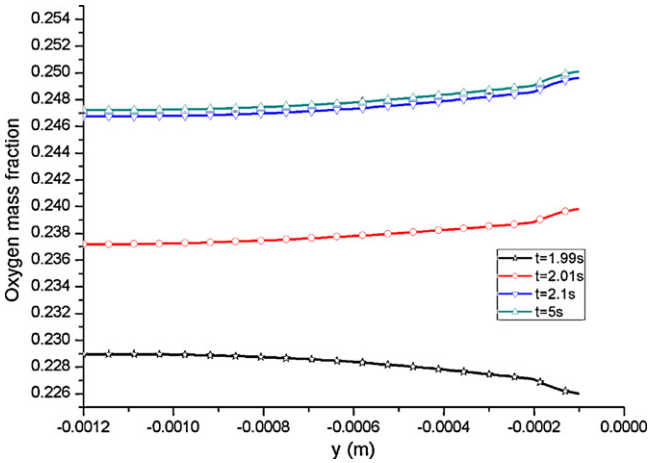

Fig. 7. Evolution history of oxygen mass fraction distribution along B–B.

from the channel towards the electrode/electrolyte interface. At the 2.01st, the overall O_2 mass fraction increases meanwhile the trend of the distribution flips, which increases from the channel towards the electrode/electrolyte interface due to the fact that the cell starts to generate oxygen. At the 2.1st, the cell is still in transient process and the O_2 mass fraction further increases. At the 5th second, the cell reaches the steady state SOEC mode with maximum O_2 mass fraction distribution.

Fig. 8 shows the corresponding evolution histories of H_2 mass fraction distributions, which have the similar trends to those of O_2 mass fraction distributions in Fig. 7. At the 1.99th second, the cell is in SOFC mode, H_2 mass fraction shows the decreasing trend from the channel towards the electrode/electrolyte interface along B–B due to H_2 consumptions by electrochemical reactions. During the switching process from SOFC mode to SOEC mode, H_2 mass fraction distribution reverses and shows an increasing trend from the channel towards electrode/electrolyte interface at the 2.01st second. The overall H_2 mass fraction distribution increases and reaches a steady state at the 5th second.

The mass fraction distribution of water vapor in hydrogen side is shown in Fig. 9. In SOFC mode at the 1.99th second, the distribution has an increasing trend from the channel towards the electrode/electrolyte interface because water vapor is generated at this electrode. Once the cell is switched to SOEC mode, water vapor is consumed by electrochemical reactions. Consequently its distribution decreases from the channel towards the

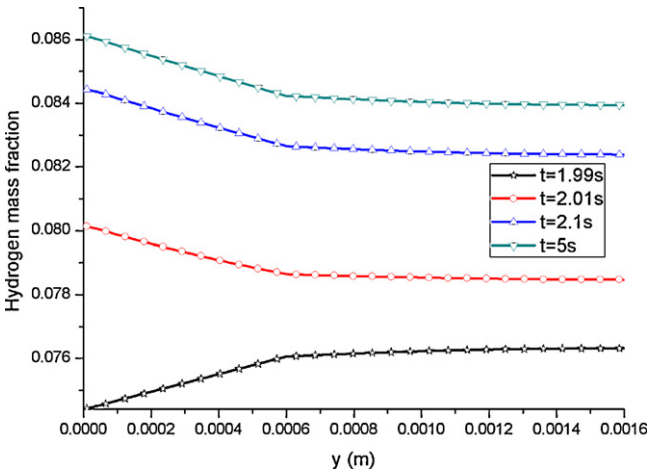

Fig. 8. Evolution history of hydrogen mass fraction distribution along B–B.

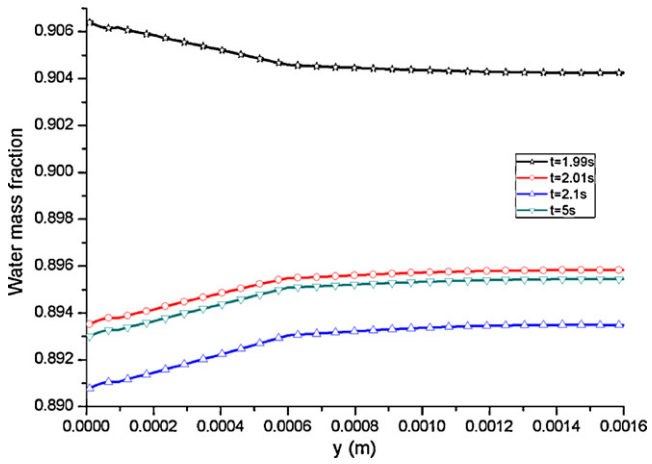

Fig. 9. Evolution history of water vapor mass fraction distribution along B–B.

electrode/electrolyte interface. Water vapor distribution keeps decreasing from the 2.01st to 2.1st second, and then increases and reaches a steady state at the 5th second. Obviously the evolution of water vapor experiences an overshoot around the 2.1st second. In comparison, H_2 mass fraction distribution in Fig. 8 does not experience such an overshoot. The reason is that H_2O is heavier than H_2, the big inertia of H_2O leads to such an overshoot phenomenon.

Fig. 10 shows the evolution history of electronic potentials along B–B. Essentially, the electronic potential at H_2 electrode keeps at

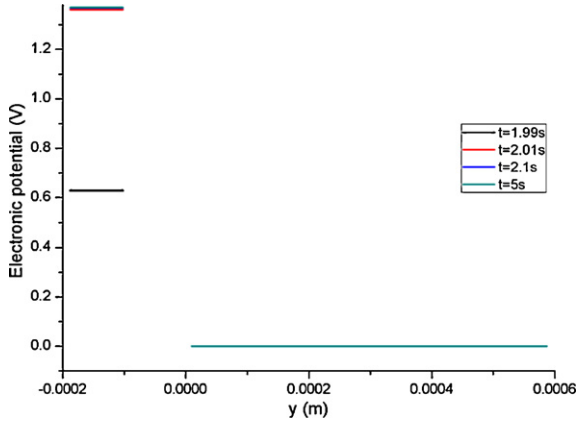

Fig. 10. Evolution history of electronic potential distribution along B–B.

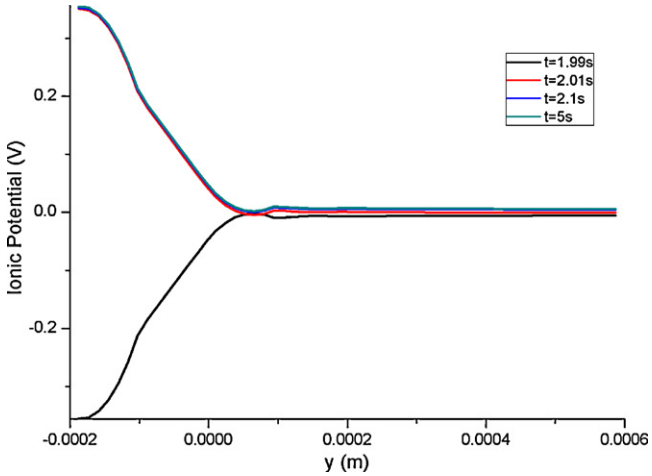

Fig. 11. Evolution history of ionic potential distribution along B–B.

0 V, while those at O_2 electrode changes. During the transient process of the mode switching, electronic potential increases from 0.62 V at SOFC mode to 1.36 V at SOEC mode and reaches maximum value at the 5th second.

Fig. 11 shows the evolutions of corresponding ionic potential distributions along B–B. At SOFC mode (1.99th second), the ionic potential at channel/O_2 electrode interface is about −0.36 V. It increases towards H_2 electrode. Beyond H_2 electrode/electrolyte interface, ionic potential keeps increasing, followed by a little bit of variations, it then reaches around 0 V. Once the operating mode starts to switch from SOFC mode at the 1.99th second to SOEC mode at the 2.01st second, ionic potential immediately flips around 0 V to positive values. During the following transient process of mode switching, ionic potentials almost keep unchanged.

5. Conclusion

In this paper, an isothermal 2D transient mathematical model is developed for solid oxide cells, which are operated in both SOFC mode and SOEC mode. The model is validated using experimental results of in-house prepared NiO–YSZ/YSZ/LSM cell under different operating temperatures. The model is employed to investigate complicated multi-physics processes during the transient process of mode switching. Simulation results indicate that the trends of internal parameter distributions, including $H_2/O_2/H_2O$ and ionic potentials, flip when the operating cell is switched from SOFC mode to SOEC mode. However, the electronic potential shows different behaviors. At H_2 electrode, electronic potential keeps at zero voltage level, while at O_2 electrode, electronic potential increases from a relatively low level in SOFC mode to a relatively high level in SOEC mode. Transient results also show that an overshoot occurs for mass fraction distribution of water vapor at H_2 side when the operating cell switches from SOFC mode to SOEC mode. The mass fractions of O_2 and H_2 as well as charge potentials (electronic and ionic) may quickly follow the operating mode changes. The simulation results presented in this paper facilitate the internal mechanism understanding for regenerative SOFCs.

Acknowledgements

This work is supported by U.S. DOE under grant no. DE-SC0001061 through Energy Frontier Research Center (EFRC) titled “Science Based Nanostructure Design and Synthesis of Heterogeneous Functional Materials for Energy Systems” and by U.S. DOE under contract no. DE-FG36-08GO88116 through the project titled “Hydrogen fuel cell development at Columbia, SC”.

References

[1] A. Boudghene Stambouli, E. Traversa, Renew. Sust. Energy Rev. 6 (5) (2002) 433–455.
[2] Y. Shi, N. Cai, C. Li, J. Power Sources 164 (2007) 639–648.
[3] M.F. Serincan, U. Pasaogullari, N.M. Sammes, J. Electrochem. Soc. 155 (11) (2008) B1117–B1127.
[4] D.H. Jeon, Electrochim. Acta 54 (2009) 2727–2736.
[5] M.M. Hussain, X. Li, I. Dincer, J. Power Sources 161 (2006) 1012–1022.
[6] Y. Shi, N. Cai, C. Li, C. Bao, E. Croiset, J. Qian, Q. Hu, S. Wang, Electrochem. Soc. 7 (1) (2007) 1889–1899.
[7] A. Chaisantikulwat, C. Diaz-Goano, E.S. Meadows, Comput. Chem. Eng. 32 (2008) 2365–2381.
[8] Y. Qi, B. Huang, K.T. Chuang, J. Power Sources 150 (2005) 32–47.
[9] X. Zhang, J. Li, G. Li, Z. Feng, J. Power Sources 163 (1) (2006) 523–531.
[10] W. Jiang, R. Fang, J.A. Khan, R.A. Dougal, J. Power Sources 162 (1) (2006) 316–326.
[11] Y.-W. Kang, J. Li, G.-Y. Cao, H.-Y. Tu, J. Li, J. Yang, J. Power Sources 188 (1) (2009) 170–176.
[12] D.F. Cheddie, N.D.H. Munroe, J. Power Sources 171 (2) (2007) 634–643.
[13] J. Li, G.-Y. Cao, X.-J. Zhu, H.-Y. Tu, J. Power Sources 171 (2) (2007) 585–600.
[14] D. Bhattacharyya, R. Rengaswamy, C. Finnerty, Chem. Eng. Sci. 64 (9) (2009) 2158–2172.

[15] J. Udagawa, P. Aguiar, N.P. Brandon, J. Power Sources 180 (2008) 46–55.
[16] J. Udagawa, P. Aguiar, N.P. Brandon, J. Power Sources 180 (2008) 354–364.
[17] J. Udagawa, P. Aguiar, N.P. Brandon, J. Power Sources 166 (2007) 127–136.
[18] M. Ni, M.K.H. Leung, D.Y.C. Leung, J. Power Sources 177 (2008) 369–375.
[19] M. Ni, M.K.H. Leung, D.Y.C. Leung, Electrochim. Acta 52 (2007) 6707–6718.
[20] M. Ni, M.K.H. Leung, D.Y.C. Leung, Int. J. Hydrogen Energy 33 (2008) 4040–4047.
[21] M. Ni, Int. J. Hydrogen Energy 34 (2009) 7795–7806.